

USING SMALL UNCREWED AIRCRAFT SYSTEMS TO EXAMINE THE SCALE DEPENDENCE OF SURFACE LAYER TURBULENCE STATISTICS OVER COMPLEX TERRAIN

Sean C.C. Bailey, Samuel C. Kever, Christina N. Vezzi, and Ryan D. Nolin
Department of Mechanical and Aerospace Engineering
University of Kentucky
Lexington, KY 40506, USA
sean.bailey@uky.edu

ABSTRACT

A series of experiments were conducted in which multiple small uncrewed aircraft systems equipped with meteorological sensors were flown over different heterogeneous terrain types in order to assess the influence of the spatial and temporal scales used for statistical calculation. The measurements are analyzed to obtain scale-dependent uncertainty estimates that can be used when employing ensemble Kalman filter approaches for assimilating measurements into numerical simulations (particularly using large-eddy simulation approaches) of micrometeorological processes. An approach is also presented that illustrates how a spectral model of turbulence can be used to model the scale dependence of the representativeness error, indicating that the representativeness error is a consequence of the boundary layer turbulence and therefore may be a significant factor when attempting to assimilate measurements taken in the boundary layer into operational simulations of low-level wind fields.

INTRODUCTION

Atmospheric boundary layer measurements of turbulent quantities are typically conducted using stationary (remote and in situ) measurement systems. As in situ measurements are often limited to sampling turbulent parameters near the surface, remote sensing systems are becoming increasingly deployed due to their ability to obtain spatially-resolved measurements. However, these systems are often expensive to install and maintain. As a result, small uncrewed aircraft systems (sUAS) are increasingly being employed in atmospheric research. sUAS have the ability to traverse through the flow spatially over time scales faster than the mean wind, allowing for a snap-shot of the turbulence structure along the flight path, and are able to measure a wide array of kinematic and thermodynamic parameters simultaneously (e.g. Egger *et al.*, 2002; Bailey *et al.*, 2019).

Recent advances in sUAS for meteorological sensing have raised interest in assimilating data from sUAS into operational weather forecasting (Jensen *et al.*, 2021, 2022). Rotorcraft sUAS in particular are attractive for these types of operations as these systems are relatively simple to operate and optimized for vertical ascent and descent. They therefore present an opportunity for low-cost, high-resolution, profiling within the planetary boundary layer and have the potential to increase fidelity of forecasts near the surface. The most practical configuration for autonomous sUAS meteorological measurements

is therefore that of a rotorcraft sUAS conducting periodic profiling at a fixed location (e.g. Chilson *et al.*, 2019). However, current rotorcraft sUAS have limited flight time and are therefore unlikely to be able to acquire statistically-converged mean profiles given the scales of turbulence in the boundary layer.

This is expected to have an impact on their use for operational meteorology. Many contemporary approaches to data assimilation employ ensemble Kalman filtering (e.g. Anderson *et al.*, 2009) to assimilate observations into forecasts, a priori knowledge of the measurement uncertainty is necessary to ensure effective assimilation of the sUAS data into numerical weather prediction (Anthes & Rieckh, 2018). Although much effort has been made to identify and minimize measurement uncertainty of the sUAS sensing elements (Barbieri *et al.*, 2019), there has been much less attention devoted to the impact of spatial heterogeneity on the representativeness error, i.e., how accurately a profile of near-surface thermodynamic and kinematic variables represents the processes within a numerical simulation grid cell. As these cells can be on the order of kilometers, and the planetary boundary layer turbulence has a Kolmogorov scale on the order of mm, the influence of boundary layer turbulence, and the boundary conditions on the turbulence, is likely to have much larger impact on the representativeness error in the boundary layer than it does in the rest of the atmosphere. There is therefore a need to quantify the influence of the representativeness error which, in turn, can be expected to depend on the temporal and spatial resolution of the numerical weather prediction.

To evaluate the uncertainty corresponding to such spatial heterogeneity, we conducted several measurements employing fixed-wing sUAS measuring the horizontal and vertical variability of temperature, moisture content, and wind over different terrain types. We then use this data to assess the temporal and spatial variability of the calculated mean value of these quantities based on the size of the statistical window used for their calculation, thereby allowing for investigation of the scale-dependence of the uncertainty associated with an assumption of horizontal homogeneity of a different measured quantities.

EXPERIMENT

To conduct the experiments, we used two or three fixed-wing BLUECAT10 sUAS simultaneously measuring over complex terrain at a single pressure altitude to obtain an estimate of the statistical variation of key properties. The BLUE-

CAT10 aircraft are commercial-off-the-shelf (COTS) vertical takeoff and landing (VTOL) configuration sUAS which have been modified to carry meteorological sensing payloads (Fig. 1), and were used in this study due to their ability to operate from an unprepared field while simultaneously providing the ability to obtain turbulence statistics over a broad horizontal extent. Each aircraft was equipped with a five-hole probe and discrete sensor package capable of measuring pressure, temperature and relative humidity (Ladino *et al.*, 2022). When combined with the kinematic aircraft velocity and orientation data sampled by the dual antenna GNSS-Aided inertial navigation system incorporated into the autopilot, this information can be refined into spatially and temporally resolved measurements of the wind vector, temperature, pressure and relative humidity through the process outlined by Van den Kroonenberg *et al.* (2008). For this study, supplementary measurements were also made by a rotorcraft and 10 m tower, but these data are not included here.

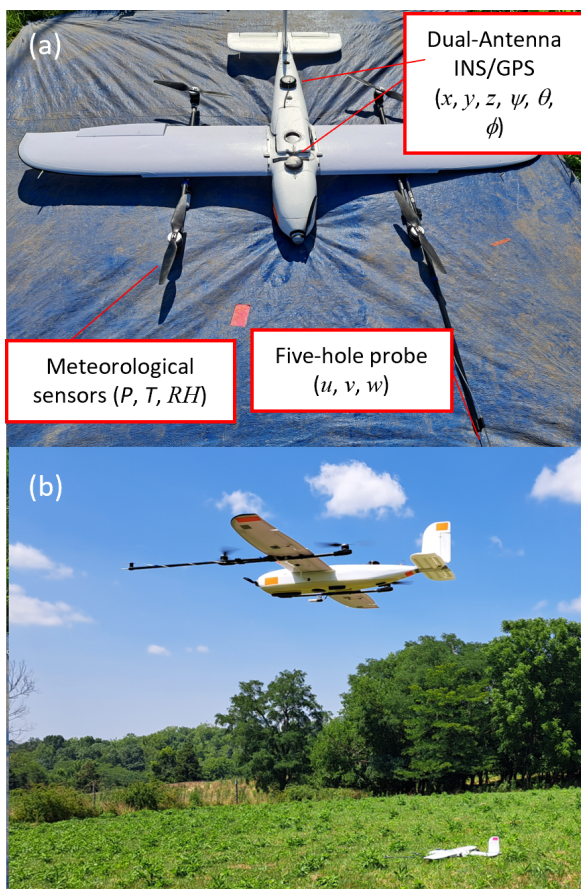


Figure 1. BLUECAT10 aircraft (a) showing location of key sensing elements and (b) VTOL takeoff.

These aircraft were used to sample the atmospheric boundary layer at two locations (Fig. 2), one with significant elevation and vegetation variability (Fig. 2a,b), and the other consisting of agricultural land use (Fig. 2c,d). The aircraft were flown autonomously following pre-programmed flight patterns consisting of rectangular trajectories at a constant pressure altitude above the launch point. Two different flight patterns were utilized, the first consisted of rectangular flight patterns were arranged with each aircraft's pattern parallel to the others, allowing for broad spatial coverage over

an approximately 1 km² area. The second consisted of the aircraft flying in square patterns with sides of approximately 500 m, with each aircraft at a different pressure altitude, such that multiple altitudes were sampled simultaneously.

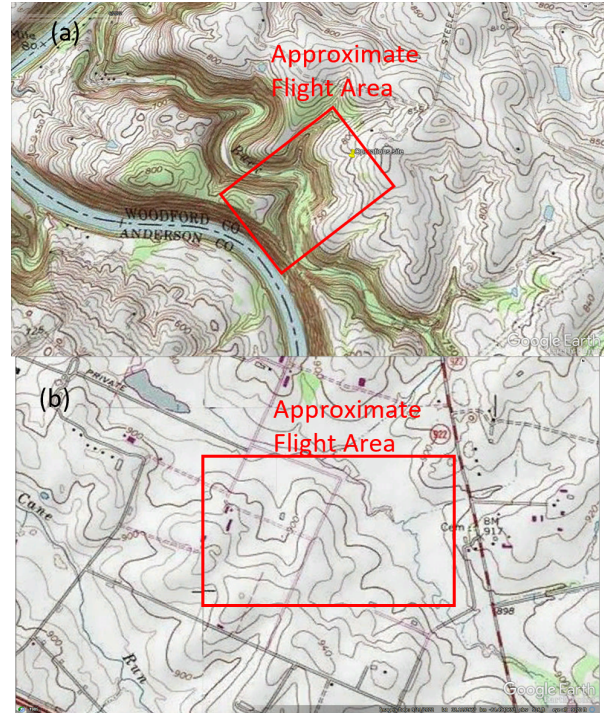


Figure 2. Topography of observation areas with (a) showing topographical map of complex terrain test site and (b) showing topographical map of agricultural test site.

Measurements were conducted for altitudes varying from $z = 50$ m above ground level (a.g.l.) to 300 m a.g.l. Measurements were also conducted during convective boundary layer conditions, such that the boundary layer conditions were relatively constant for several flights (thereby allowing for multiple samples at a single altitude, or samples to be acquired at multiple altitudes, with limited variability in boundary conditions. Additional flights were conducted over the course of a morning boundary layer transition, such that measurements could be conducted under different stability conditions.

ANALYSIS APPROACH

The objective of this analysis is primarily to determine the uncertainty associated with the assumption that a statistical observation made by profiling at particular spatial location is homogeneous throughout a numerical grid cell and time step. In other words, the analysis seeks to investigate the spatial and temporal scale dependence of statistics measured in heterogeneous boundary conditions. We simplify the problem to a single spatial direction, and use each straight line segment of the flight path as an individual member of an ensemble of measurements along the horizontal direction. Each member of the ensemble could then be divided into M samples of length, Δx (note that as Δx increases, the number of samples obtained during each flight necessarily decreases using this approach).

This approach was then extended into the temporal domain by treating each member of the ensemble as being separated by a time separation of δt . The flight could then be

divided sample sizes of duration $\Delta t = p\delta t$, with p being the number of ensemble members included in the calculation. The total number of samples, N , is therefore determined by the overall duration of the flight, divided by Δt .

Scale-dependent statistics could then be calculated for each flight. For example, the Δx - and Δt -dependent average value of a quantity Φ , here written as $\overline{\Phi}(\Delta x, \Delta t)$ can be found from

$$\overline{\Phi}(\Delta x, \Delta t) = \frac{1}{M} \frac{1}{N} \sum_{m=1}^M \sum_{n=1}^N \langle \Phi \rangle(\Delta x_m, \Delta t_n) \quad (1)$$

where m and n are indices for each sample of $\Phi(\Delta x_m, \Delta t_n)$ and $\langle \Phi \rangle(\Delta x_m, \Delta t_n)$ is the mean value obtained for each sample.

Of particular interest, however, is the scale-dependent variability of different statistical quantities (e.g. the mean value of wind magnitude, $\langle U \rangle$), which we use here as a proxy for the uncertainty associated with the scales Δx and Δt over which $\langle U \rangle$ is determined. This variability can be quantified by

$$\sigma_{\Phi}^2(\Delta x, \Delta t) = \frac{1}{M} \frac{1}{N} \sum_{m=1}^M \sum_{n=1}^N \langle \Phi^2 \rangle(\Delta x_m, \Delta t_n) \quad (2)$$

where $\langle \Phi^2 \rangle$ is the variance calculated for each sample $\Phi(\Delta x_m, \Delta t_n)$.

To present these results as an uncertainty, we normalize these quantities measured as a function of Δx and Δt by the same statistic calculated over scales of Δx_0 and Δt_0 , which represent the spatial and temporal scales sampled at the same altitude by a vertically profiling aircraft. In this way, $2\overline{\Phi^2}^{1/2}(\Delta x, \Delta t)/\overline{\Phi}(\Delta x_0, \Delta t_0)$ represents a scale-dependent $\pm 95\%$ uncertainty estimate, with spatial scales represented by Δx and temporal scales by Δt . These scales then act as analogues to a numerical horizontal mesh size and time step.

Example distributions of this uncertainty estimate, representing the uncertainty associated with the assumption of a homogeneous distribution of mean wind velocity magnitude are provided in Figure 3(a) and (b) for the complex and agricultural topographies, respectively. Similar surfaces were measured for both measurement sites, with the more homogeneous topography surprisingly producing slight higher uncertainty estimates. The results shown in Figure 3(a) and (b) indicate that the uncertainty associated with assuming a single profile measurement of wind velocity magnitude is a valid representation of the mean value of a mesh scale and time step of Δx and Δt , can reach values up to 45% if the numerical time step is $\Delta t = 25$ minutes and the cell dimensions are of the order $\Delta x = 500$ m.

More importantly, the form of the uncertainty surfaces presented Figure 3(a) and (b) suggests that a model can be developed to represent this uncertainty dependence by assuming all variability arises due to sub- Δx - and sub- Δt -scale turbulent fluctuations within the numerical mesh. The starting point for this model is a traditional spectral model, for example such as presented by Pope (2000) which builds on the inertial cascade/dissipation range of the Pao/Kolmogorov spectrum with a modification to model the energy containing range

$$E(\kappa) = C\varepsilon^{2/3} \kappa^{-5/3} f_L(\kappa L) f_\eta(\kappa \eta) \quad (3)$$

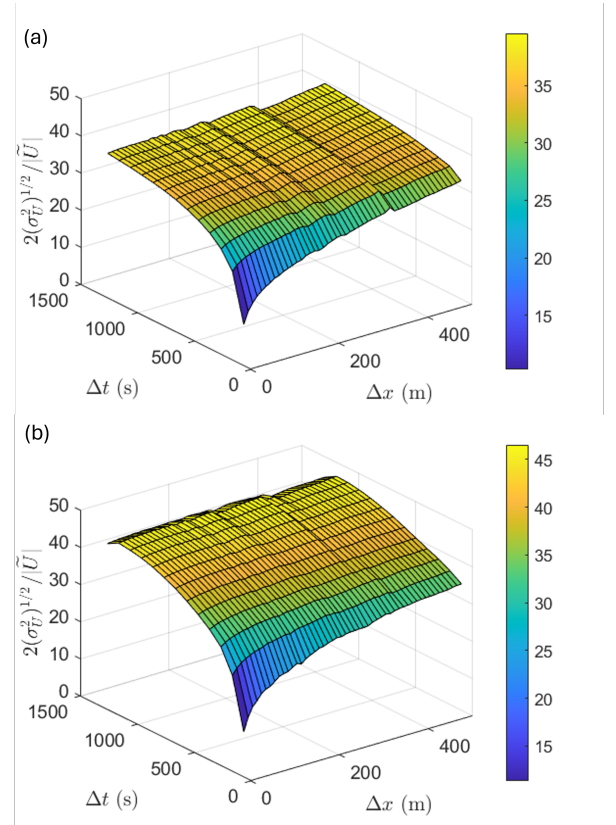


Figure 3. Estimated uncertainty in % and its dependence on spatial (Δx) and temporal (Δt) scales used for the calculation of mean wind velocity magnitude for (a) complex topography and (b) agricultural topography.

where κ is the three-dimensional wavenumber and

$$f_L(\kappa L) = \left(\frac{\kappa L}{[(\kappa L)^2 + c_L]^2} \right)^{5/3+p_0} \quad (4)$$

and

$$f_\eta(\kappa \eta) = \exp \left(-\beta \left([(\kappa \eta)^4 + c_\eta^4]^{1/4} - c_\eta \right) \right) \quad (5)$$

represent modifications to the Kolmogorov inertial subrange to approximate the energy-containing and dissipative ranges respectively. In these equations $C = 1.5$, $c_L = 6.78$ and $c_\eta = 0.4$, L is an integral scale, and η is the Kolmogorov microscale.

As the measured velocity is only known along a linear path, we also need to convert the three-dimensional spectrum to a one-dimensional spectrum following

$$E_{\ell\ell}(\kappa_\ell) = \int_{\kappa_\ell}^{\infty} \frac{E(\kappa)}{\kappa} \left(1 - \frac{\kappa_\ell^2}{\kappa^2} \right) d\kappa \quad (6)$$

where κ_ℓ is the component of the wavenumber vector in the longitudinal direction.

This model therefore allows the quantification of turbulent fluctuations contained within a wavenumber range of $\Delta \kappa_\ell \rightarrow \infty$ (equivalent to the spatial range $\sim 0 < \Delta x / 2\pi$), which

can be done using

$$\sigma_{\vec{U}}^2(\Delta\kappa_\ell) = \int_{\Delta\kappa_\ell}^{\infty} E_{\ell\ell}(\kappa_\ell) d\kappa_\ell. \quad (7)$$

To apply this model to the uncertainty analysis, which is a function of Δx and Δt we must first translate Δt to the wavenumber domain using Taylor's hypothesis such that $\Delta x_2 \approx U\Delta t$. In this way we can find $\Delta x = (\Delta x_1 + \Delta x_2^2)^{1/2}$, where Δx_1 is the spatial separation in the wavenumber domain. This result lets us find $\Delta\kappa_\ell \approx 2\pi/\Delta x$ and hence $\overline{U^2}(\Delta x, \Delta t)$ through equation 7.

However, to do so, we must first quantify L , ε and η . To determine ε for each flight, $E_{\ell\ell}(\kappa_\ell)$ was estimated using the component of the wind velocity aligned with the wind direction relative to the aircraft trajectory. This was calculated by first rotating the measured wind vector, $\vec{U} = (u, v, w)$, from the meteorological east-north-up wind coordinate system to instead align u with an axis parallel to the velocity of the aircraft within the air, i.e. we define $u_\ell(t)$ as the component of the wind velocity vector in the direction of the mean velocity of the air relative to the aircraft. The velocity spectrum of $u_\ell(t)$ in the frequency domain, $F_{\ell\ell}(f)$, was then calculated on this rotated wind velocity vector. Noting that since the spectral model is defined in the wavenumber domain, $F_{\ell\ell}(f)$ was then transformed to $E_{\ell\ell}(\kappa_\ell)$. To do this, the longitudinal wavenumber, κ_ℓ , was approximated using Taylor's frozen-flow hypothesis such that $\kappa_\ell \approx f2\pi|\vec{V}_R|^{-1}$, where \vec{V}_R is the relative wind velocity vector. We then found the longitudinal velocity spectrum in the wavenumber domain as $E_{\ell\ell} = F_{\ell\ell}|\langle\vec{V}_R\rangle|(2\pi)^{-1}$.

Finally,

$$E_{\ell\ell}(\kappa_\ell) = 0.49\varepsilon^{2/3}\kappa_\ell^{-5/3} \quad (8)$$

was used to estimate ε by least-squares fit of the measured $(E_{\ell\ell}\kappa_\ell^{5/3}/0.49)^{3/2}$ over the κ_ℓ range corresponding to the inertial subrange. The result is an estimate of ε for each member of the ensemble, which could then be used to provide an averaged value for the entire flight. In this way

$$\eta = \left(\frac{v^3}{\varepsilon}\right)^{1/4} \quad (9)$$

and

$$L = \frac{k^{3/2}}{\varepsilon} \quad (10)$$

can be determined, where $k = 0.5(\overline{u^2} + \overline{v^2} + \overline{w^2})$ is the turbulent kinetic energy measured during each flight.

Sample results from the measured values of k and ε are shown in Fig. 4(a) and (b) for flights conducted at $z = 50$ m, 150 m and 300 m over the course of a morning boundary layer transition. Not surprisingly, the two quantities follow approximately the same trends, with the profiles measured at 11:00 UTC, and 12:00 UTC (when the boundary layer was stable) showing relatively low values of $k \approx 0.075$ m²/s² and $\varepsilon \approx 0.0001$ m²/s³. As the boundary layer transitions to becoming unstable and convective, the turbulence increases near the surface first, as shown in the 13:00 UTC profiles, but then

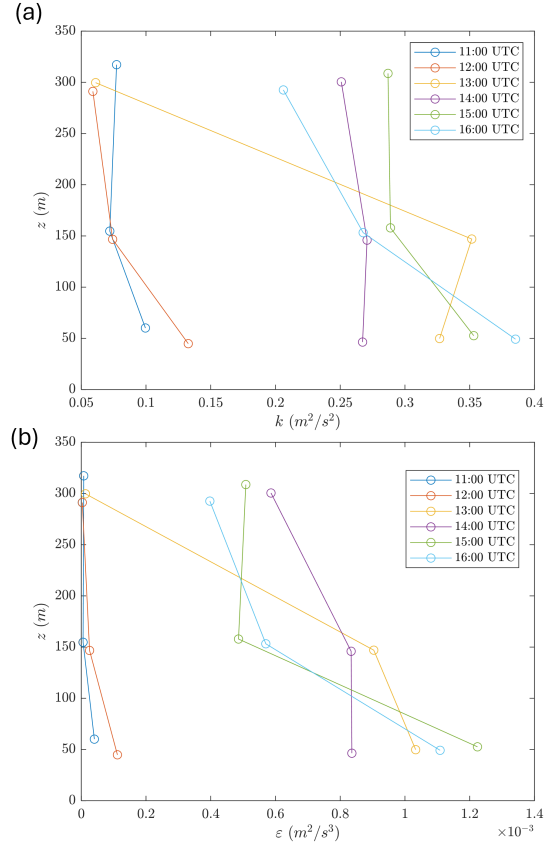


Figure 4. (a) Turbulent kinetic energy and (b) turbulent kinetic energy dissipation rate measured as a function of altitude and time of day. For this measurement, the atmospheric boundary layer transitions from stable to convective conditions between 12:00 UTC and 14:00 UTC.

expands to the entire boundary layer, such that 15:00 UTC $k \approx 0.35$ m²/s² and $\varepsilon \approx 0.0012$ m²/s³ near the surface.

When combined to produce an estimated integral length scale, $L = k^{3/2}/\varepsilon$, as done in Fig 5(a), the integral scales are found to be very large when the boundary layer is stable, on the order of a 1 km for profiles measured before 13:00 UTC, decreasing to $L \approx 200$ m for the convective conditions. The corresponding Kolmogorov scale, shown in Fig 5(b), varies between 6 mm and 1.5 mm over the same time period.

When the k and ε measured during the flights corresponding to Fig. 3(a) and (b) are used to model the scale-dependent velocity variance through equations 3 to 7, the corresponding estimate of representativeness error can be determined as $2(\sigma_{\vec{U}}^2)^{1/2}/|U|$. The dependence of this value on Δx and Δt is shown in Fig. 6(a) and (b) for the conditions equivalent to those shown in Fig. 3(a) and (b).

It is apparent that the scale dependence of the modeled representativeness error accurately captures the corresponding scale dependence of the measured results. Hence, considering that both complex and agricultural topography are represented, the representativeness error within the boundary layer can be approximated as a manifestation of the turbulence that is produced by the terrain and can be expected to therefore depend on local boundary conditions, including the balance between mechanical and buoyant turbulent production.

However, there are some structural differences that can be observed between Figs. 6 and 3, including the overall magnitude of the modeled representativeness error. Notably, the

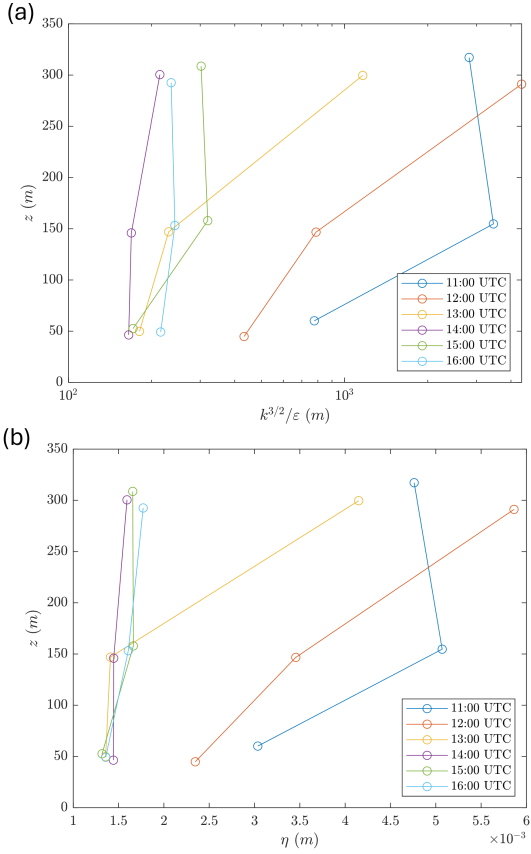


Figure 5. (a) Estimated integral length scale and (b) Kolmogorov length scale derived from k and ε measured as a function of altitude and time of day. For this measurement, the atmospheric boundary layer transitions from stable to convective conditions between 12:00 UTC and 14:00 UTC.

maximum modeled representativeness error for the complex terrain is 40%, which corresponds to the maximum measured value (occurring at the largest Δx and Δt) for the same case. However, for the agricultural case, the modeled error maximum is 35%, whereas the measured value was closer to 45%. It is suspected that this may be due to inaccuracy in the determination of k and ε from the sUAS measurements and further work is being conducted to refine these estimates.

Regardless, the results shown in Fig. 6 are promising, and suggest that the approach presented in equations 3 through 7 can provide reasonable estimates of representativeness error for use in operational data assimilation. To expand this model to the scalars corresponding to heat and moisture content, we can treat them as being passively transported by the turbulence. If this is the case, then a similarly structured wavenumber spectrum should exist for concentration of the scalar (e.g. heat and moisture), with an inertial subrange analog to Kolmogorov’s inertial cascade. If we assume that the ratio of scalar-to-momentum fluctuations in the inertial subrange persists throughout the entire wavenumber range, then we can scale the turbulent model for wind velocity fluctuations to model the fluctuations of different passive scalars. Preliminary results (not shown) suggest that this approach produces reasonable approximations of the scale-dependent uncertainty of temperature and vapor mixing ratio, although further work is required to correctly capture the amplitude of the error.

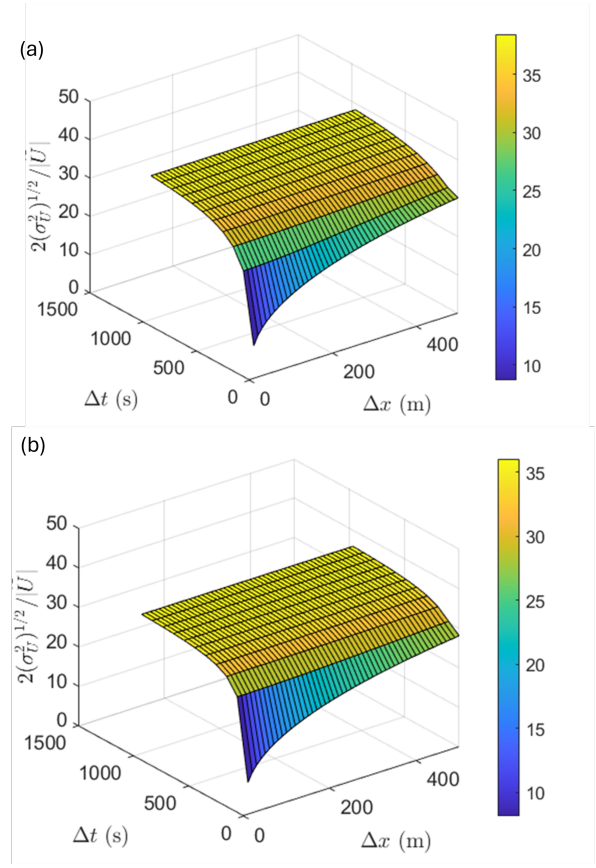


Figure 6. Estimated 95% error of U (in percent of absolute value) modeled from k and ε as a function of Δx_1 and Δt . Different surfaces represent different transect directions for each aircraft.

CONCLUSIONS

The results of this study suggest that it is possible to model the influence of boundary conditions on the uncertainty associated with assuming a single measured profile represents the average value within a numerical grid cell at a single time step. Although only results for mean velocity have been presented here, this process can be extended to scalar values (e.g. temperature and moisture content) by using similar spectral models for these quantities. Additionally, measurements conducted to assess the influence of altitude and boundary layer stability on these uncertainty measurements, have shown that boundary layer stability plays a significant role on the representativeness error, with stable conditions resulting in negligible representativeness error.

The objective of these measurements is to develop an uncertainty model which can be implemented in ensemble Kalman filter data assimilation schemes as employed in large eddy simulations of micrometeorological and atmospheric boundary layer processes. In this regard, the approach presented would be implemented by using the estimated values of turbulent kinetic energy and dissipation rate, extracted from the numerical prediction itself. Additional work will be required to determine if proxy Kolmogorov and integral length scales can be used for numerical simulations where this information is not readily available.

REFERENCES

- Anderson, Jeffrey, Hoar, Tim, Raeder, Kevin, Liu, Hui, Collins, Nancy, Torn, Ryan & Avellano, Avelino 2009 The data assimilation research testbed: A community facility. *Bulletin of the American Meteorological Society* **90** (9), 1283–1296.
- Anthes, Richard & Rieckh, Therese 2018 Estimating observation and model error variances using multiple data sets. *Atmospheric Measurement Techniques* **11** (7), 4239–4260.
- Bailey, Sean C. C., Canter, Caleb A., Sama, Michael P., Houston, Adam L. & Smith, Suzanne Weaver 2019 Unmanned aerial vehicles reveal the impact of a total solar eclipse on the atmospheric surface layer. *Proceedings of the Royal Society A: Mathematical, Physical and Engineering Sciences* **475** (2229), 20190212.
- Barbieri, Lindsay, Kral, Stephan T., Bailey, Sean C. C., Frazier, Amy E., Jacob, Jamey D., Reuder, Joachim, Brus, David, Chilson, Phillip B., Crick, Christopher, Detweiler, Carrick, Doddi, Abhiram, Elston, Jack, Foroutan, Hosein, González-Rocha, Javier, Greene, Brian R., Guzman, Marcelo I., Houston, Adam L., Islam, Ashraful, Kempinen, Osku, Lawrence, Dale, Pillar-Little, Elizabeth A., Ross, Shane D., Sama, Michael P., Schmale, David G., Schuyler, Travis J., Shankar, Ajay, Smith, Suzanne W., Waugh, Sean, Dixon, Cory, Borenstein, Steve & de Boer, Gijs 2019 Intercomparison of small unmanned aircraft system (suas) measurements for atmospheric science during the lapse-rate campaign. *Sensors* **19** (9).
- Chilson, Phillip B, Bell, Tyler M, Brewster, Keith A, Britto Hupsel de Azevedo, Gustavo, Carr, Frederick H, Carson, Kenneth, Doyle, William, Fiebrich, Christopher A, Greene, Brian R, Grimsley, James L *et al.* 2019 Moving towards a network of autonomous uas atmospheric profiling stations for observations in the earth’s lower atmosphere: The 3d mesonet concept. *Sensors* **19** (12), 2720.
- Egger, J., Bajrachaya, S., Heingrich, R., Kolb, P., Lammlein, S., Mech, M., Reuder, J., Schäper, W., Shakya, P., Shween, J. & H., Wendt. 2002 Diurnal winds in the himalayan kali gandaki valley. part iii: Remotely piloted aircraft soundings. *Mon. Wea. Rev.* **130**, 2042–2058.
- Jensen, Anders A, Pinto, James O, Bailey, Sean CC, Sobash, Ryan A, de Boer, Gijs, Houston, Adam L, Chilson, Phillip B, Bell, Tyler, Romine, Glen, Smith, Suzanne W *et al.* 2021 Assimilation of a coordinated fleet of uncrewed aircraft system observations in complex terrain: Enkf system design and preliminary assessment. *Monthly Weather Review* **149** (5), 1459–1480.
- Jensen, Anders A, Pinto, James O, Bailey, Sean CC, Sobash, Ryan A, Romine, Glen, Boer, Gijs de, Houston, Adam L, Smith, Suzanne W, Lawrence, Dale A, Dixon, Cory *et al.* 2022 Assimilation of a coordinated fleet of uncrewed aircraft system observations in complex terrain: Observing system experiments. *Monthly Weather Review* **150** (10), 2737–2763.
- Van den Kroonenberg, Aline, Martin, Tim, Buschmann, Marco, Bange, Jens & Vörsmann, Peter 2008 Measuring the wind vector using the autonomous mini aerial vehicle m2av. *Journal of Atmospheric and Oceanic Technology* **25** (11), 1969–1982.
- Ladino, Karla S, Sama, Michael P & Stanton, Victoria L 2022 Development and calibration of pressure-temperature-humidity (pth) probes for distributed atmospheric monitoring using unmanned aircraft systems. *Sensors* **22** (9), 3261.
- Pope, S. B. 2000 *Turbulent Flows*. Cambridge University Press.